Computer Physics Communications 80 (1994) 145–167
North-Holland

Computer Physics Communications

Multiphonon atom–surface scattering

Joseph R. Manson
Department of Physics and Astronomy, Clemson University, Clemson, SC 29634, USA

We consider the interaction of a neutral atom colliding with a solid surface and develop a general quantum mechanical theory describing the multiphonon inelastic transfer processes to arbitrarily high order in numbers of exchanged phonons. Starting from general principles of formal scattering theory the trajectory approximation to the scattering intensity is developed. From the trajectory approximation it is shown that a fast collision approximation is applicable when the multiphonon exchange is dominated by small frequency and long wavelength phonons. The semiclassical and classical limits are developed. Numerical calculations produce good agreement with a variety of experiments for conditions ranging from the quantum mechanical regime to nearly classical scattering.

1. Introduction

The scattering of small mass and low energy neutral atoms has for many years been of interest as a method of obtaining information about fundamental physical processes occurring at surfaces. Interest in this field of study was initially sparked by the seminal experiments of Stern and coworkers [1–4] who used a thermal beam of He atoms diffracting from a cleaved LiF(001) surface to verify the De Broglie hypothesis for the wave-like nature of a particle. This work very quickly stimulated a large degree of theoretical interest [5–14], virtually all of which was carried out within the framework of what is now known as the distorted wave Born approximation.

In the late 1960's and early 1970's advances in vacuum technology, and especially the development of extremely monoenergetic molecular jet beams of thermal energy particles, stimulated a new round of experimental activity [15–19] which has continued unabated to the present time. These experiments were quickly followed by renewed theoretical interest [20–22]. More recent experimental and theoretical developments have been discussed in a number of excellent review articles in the last few years [23–30].

Current state-of-the-art experiments consist of a monoenergetic jet beam incident on the surface and a time-of-flight scattered intensity detector capable of resolving the energy as well as the polar and azimuthal angles of the scattered particles. All of this equipment is contained in an ultra-high vacuum chamber in order to maintain the cleanliness of the surface. The characteristic features of the scattered intensity can be roughly grouped into four components: elastic diffraction peaks arising as a result of the underlying periodicity of the crystal substrate, the diffuse elastic intensity caused by defects, single surface phonon peaks, and the diffuse inelastic background. The elastic diffraction peaks are the easiest to interpret as their positions are determined by the periodicity of the crystal surface. The intensities of these diffraction peaks relative to the incident beam, when compared with calculations, give the corrugation of the surface potential as observed by the scattering projectiles. Broadening and shifts in position of the diffraction peaks indicate deviations from perfect periodicity in the surface. The diffuse

Correspondence to: J.R. Manson, Department of Physics and Astronomy, Clemson University, Clemson, SC 29634, USA.

SSDI 0010-4655(93)E104-U

elastic peak appears at all scattering angles and is due to symmetry-breaking impurities and imperfections on the surface. Its origins are less well understood than the diffraction, although it has been shown to yield important information about the differential cross section of defects [31–33] or adsorbates [34] on the surface. The single phonon peaks arise from single quantum inelastic interactions with phonon modes which are localized in the surface region. These include surface modes associated with a perfect crystal, such as Rayleigh phonons, and also other excitations such as modes due to surface adsorbates. These single phonon intensities are relatively well understood [29] and tractable calculations can be readily carried out [35].

The main object of interest in this paper is the diffuse inelastic intensity which appears as a broad background in the experimental time-of-flight measurements, especially at higher incident beam energies and elevated surface temperatures. The diffuse inelastic background consists of two parts, incoherent inelastic scattering from defects [36] and the coherent multiphonon contribution. For clean, well ordered surfaces the multiphonon contribution usually dominates, and although diffuse, it is not featureless. Structure appears in the multiphonon contribution and peaks can occur which resemble single phonon features [37], thus for this reason alone it is important to have a good understanding of these processes. A good knowledge of the form and shape of the diffuse inelastic signal is essential for background subtraction in order to obtain the true values of the elastic and single surface phonon peaks. However, the inelastic background contains far more interesting physical information than simply that necessary for background subtraction. We will show that it provides important information on the interaction potential which couples the projectile to the surface, and the large range of experimental conditions currently available provide excellent examples of the transition from the quantum mechanical regime to the classical scattering regime.

There have been a number of general approaches to the inelastic surface scattering problem that are capable in principle of describing the complete picture of multiquantum exchanges upon collision [38–55], most of which involve semiclassical approximations or at least invoke some form of the trajectory approximation [56–59]. Actual quantitative calculations of the multiquantum scattered intensities for direct comparison with experiment have generally proven to be difficult and cumbersome to carry out.

In this paper we review and develop a complete and formally exact treatment of the general surface scattering problem. We then sequentially apply the trajectory approximation and the semiclassical approximation in order to make the connection with several of the previous theoretical treatments. We show that under conditions in which the multiphonon intensity is dominated by interactions with quanta whose energies and wavevectors are small, conditions which are very broadly applicable, a quick collision approximation can be applied which leads to expressions which can readily be calculated. Finally, we show a number of comparisons with experiment illustrating the usefulness of this approach.

In the next section we develop the formal theory of the interaction of an atomic projectile with the surface including a complete picture of the interactions with the surface vibrational modes. In section 3 below we develop the trajectory approximation and in section 4 we develop the quick collision approximation and conditions for which it is valid, as well as making the connection to various levels of the semiclassical approximation. Section 8 presents the results of several representative comparisons with recent experiments spanning the range of conditions from very quantum mechanical scattering to near classical scattering. In section 9 we draw a number of conclusions from this work.

2. Formal development

The interaction between the atomic projectile and the surface can be described by a Hamiltonian of the form

$$H = H^{\mathrm{p}} + H^{\mathrm{c}} + V, \tag{1}$$

where H^{p} is the Hamiltonian of the free particle, H^{c} is the Hamiltonian of the unperturbed crystal, and V is the interaction coupling the projectile and crystal. A standard approach is to start from the probability density of the particle to lose an amount of energy E given by [50,56]

$$N(E) = \langle\langle (n_i, \boldsymbol{k}_i | S^{\dagger}\, \delta(H^{\mathrm{p}} - E_i^{\mathrm{p}} + E)\; S | \boldsymbol{k}_i, n_i) \rangle\rangle, \tag{2}$$

where the symbol $\langle\langle\ \rangle\rangle$ defines an ensemble average over the initial crystal states $|n_i)$, and the scattering operators S are defined by

$$S = \lim_{t \to \infty} U(-t, t), \tag{3}$$

where $U(s_1, s_2)$ is the time evolution operator. Global energy conservation between projectile and crystal allows us to replace the energy δ-function by one involving the crystal Hamiltonian, $\delta(H^{\mathrm{c}} - E_i^{\mathrm{c}} - E)$.

Following the approach of Brako and Newns [42,43] and of Bortolani and Levi [25], it is convenient for considerations of parallel momentum exchange to consider the probability density of exchanging, between particle and crystal, both an amount E of energy and an amount $\hbar\boldsymbol{K}$ of parallel momentum. Such a probability density is defined by

$$P(\boldsymbol{K}, \Delta) = \frac{1}{\hbar^2} \sum_{\boldsymbol{G}} \langle\langle (n_i, \boldsymbol{k}_i | S^{\dagger}\, \delta(H^{\mathrm{c}} - E_i^{\mathrm{c}} - E)\; \delta(\hat{\boldsymbol{K}}^{\mathrm{c}} - \boldsymbol{K}^{\mathrm{c}} + \boldsymbol{K} + \boldsymbol{G})\; S | \boldsymbol{k}_i, n_i) \rangle\rangle, \tag{4}$$

where $\hbar\hat{\boldsymbol{K}}^{\mathrm{c}}$ is the momentum operator for the crystal, and the sum over reciprocal lattice vectors $\boldsymbol{G}$ appears because momentum is not conserved in the collision. The differential reflection coefficient, which is usually compared to the experimentally measured intensities, is related to eq. (4) by a simple density of states:

$$\frac{\mathrm{d}R}{\mathrm{d}\Omega_f\, \mathrm{d}E} = \hbar^2 k_f k_{fz} P(\boldsymbol{K}, E), \tag{5}$$

where $\hbar\boldsymbol{k}_f$ is the final projectile momentum and $\hbar k_{fz}$ is its component in the direction normal to the surface. The delta functions in eq. (4) are rewritten as integral representations [60] in the transformation usually ascribed to Glauber [61,62] and Van Hove [63], and after defining time-dependent operators in a generalized interaction picture according to

$$S(\boldsymbol{R}, t) = \mathrm{e}^{-\mathrm{i}(\boldsymbol{R}\cdot\hat{\boldsymbol{K}}^{\mathrm{c}} - H^{\mathrm{c}} t/\hbar)} S\, \mathrm{e}^{\mathrm{i}(\boldsymbol{R}\cdot\hat{\boldsymbol{K}}^{\mathrm{c}} - H^{\mathrm{c}} t/\hbar)}, \tag{6}$$

the differential reflection coefficient appears in the general form

$$\frac{\mathrm{d}R}{\mathrm{d}\Omega_f\, \mathrm{d}E} = \frac{k_f k_{fz}}{(2\pi)^3 \hbar L^2} \sum_{\boldsymbol{G}} \int_{-\infty}^{+\infty} \mathrm{d}t \int \mathrm{d}\boldsymbol{R} \int \mathrm{d}\boldsymbol{R}'\, \exp\{\mathrm{i}[(\boldsymbol{K} + \boldsymbol{G}) \cdot (\boldsymbol{R} - \boldsymbol{R}') - Et/\hbar]\}$$
$$\times \langle\langle (n_i, \boldsymbol{k}_i | S^{\dagger}(\boldsymbol{R}, 0) \boldsymbol{k}_f)(\boldsymbol{k}_f | S(\boldsymbol{R}', t) \boldsymbol{k}_i, n_i) \rangle\rangle. \tag{7}$$

Equation (7) is formally without approximation, and is a quite general expression for describing the scattering. However, in order to make progress towards tractable calculations, approximations must be applied. The scattering operator $S(\alpha)$ can be represented in several forms, but perhaps the most convenient for the later introduction of approximations is the time-dependent exponential in the interaction picture [64]

$$S(\alpha) = \mathscr{T} \lim_{t_0 \to \infty} \exp\left[(-\mathrm{i}/\hbar) \int_{-t_0}^{+t_0} V(\alpha; t)\, \mathrm{d}t \right], \tag{8}$$

where $\alpha = (\boldsymbol{R}, t)$ signifies the supplementary variables of the driving operators as in eq. (6) and $\mathscr{T}$ is the time ordering operator. When (8) is inserted into (7), even very severe approximations applied to the many-body potential V will often result in a final expression for the scattering probability which still obeys the condition of unitarity. This will be the starting point for further development.

3. Trajectory approximation

The trajectory approximation consists in assuming that the projectile follows a classical trajectory from its initial state characterized by momentum $\hbar \boldsymbol{k}_i$ to its final state $\hbar \boldsymbol{k}_f$. An alternative way of arriving at the trajectory approximation is to set up the scattering problem in the Feynman path integral formalism, and then limit the number of paths to one classically allowed path (or in some cases a small number of paths). Although the particle moves along a classical trajectory, it is still possible to consider its further interactions with the crystal, in particular the inelastic exchange of quanta, in a completely quantum mechanical manner. Another useful approximation that has often been applied to inelastic scattering is the semiclassical approximation. The semiclassical approximation has several different forms but usually it consists of imposing the further restriction that the final and initial energies of the projectile are not appreciably different, as expressed by the relation $k_f \approx k_i$.

We will develop the trajectory approximation directly from eq. (7). We first need to discuss the interaction potential $V = V(\boldsymbol{r}, \{\boldsymbol{u}\})$ where $\{\boldsymbol{u}\}$ symbolizes the set of displacement variables of the crystal. Since the atomic projectiles do not scatter directly from the crystal atoms, rather they are scattered by the weak electron cloud in front of the surface, it may be much more useful to divide the unit cell up into divisions other than those usually associated directly with the atomic cores.

We write the interaction potential as the sum of two parts

$$V = V^0 + V^1, \tag{9}$$

where the "strong" part V^0 contains the terms which backscatter the projectile and prevent it from penetrating appreciably into the bulk, and the remainder V^1 contains the major terms describing interactions with the lattice vibrations. If the potential is expanded in a Taylor series in the lattice vibrations, then

$$V = V(\boldsymbol{r}, \{\boldsymbol{u}_{j,\kappa}\})\Big|_{\boldsymbol{u}_{j,\kappa}=0} + \sum_{j,\kappa} \boldsymbol{u}_{j,\kappa} \cdot \boldsymbol{\nabla}_{j,\kappa} V(\boldsymbol{r}, \{\boldsymbol{u}_{j,\kappa}\})\Big|_{\boldsymbol{u}_{j,\kappa}=0} + \cdots, \tag{10}$$

where $\boldsymbol{\nabla}_{j,\kappa}$ is the gradient operator with respect to the (j, κ) displacement. We use a notation for the set of indices (j, κ), in which j is a two-dimensional variable that counts unit cells of the surface and κ is three-dimensional and counts elements of the basis set within the unit cell including those in all the layers below the surface. Usually κ counts the crystal atoms making up the basis set of the unit cell, but we note that this does not necessarily need to be the case. The logical choice is to associate V^0 with the leading term of (10) which is now independent of the displacement, and let V^1 be the sum of all higher order terms. A great simplification occurs in the case in which the potential is a summation of pairwise atomic interactions:

$$V = \sum_{j,\kappa} v(\boldsymbol{r} - \boldsymbol{r}_j - \boldsymbol{r}_\kappa - \boldsymbol{u}_{j,\kappa}), \tag{11}$$

where the position of the (j, κ) element in the lattice as a function of time is written as $\boldsymbol{r}_{j,\kappa}(t) = \boldsymbol{r} + \boldsymbol{r}_j + \boldsymbol{r}_\kappa + \boldsymbol{u}_{j,\kappa}(t)$ with $\boldsymbol{r}_j$ and $\boldsymbol{r}_\kappa$ the equilibrium positions of the jth unit cell and the κth element within the

cell, respectively. Then

$$V = \sum_{j,\kappa} v(\boldsymbol{r} - \boldsymbol{r}_j - \boldsymbol{r}_\kappa) - \nabla_r \cdot \sum_{j,\kappa} v(\boldsymbol{r} - \boldsymbol{r}_j - \boldsymbol{r}_\kappa)\boldsymbol{u}_{j,\kappa} + \cdots$$
$$= V^0 + \sum_{j,\kappa} \boldsymbol{f}_{j,\kappa} \cdot \boldsymbol{u}_{j,\kappa} + \cdots, \tag{12}$$

where we have made the further association that $\boldsymbol{f}_{j,\kappa} = -\nabla_r v(\boldsymbol{r} - \boldsymbol{r}_j - \boldsymbol{r}_\kappa)$ is the classical force on the projectile due to the (j, κ) crystal atom.

However, separation of the form of (10) or (12) is certainly not unique, and for certain purposes it may be more convenient to make the distinction between displacements of the unit cell taken as a whole and the additional displacements within the basis. For example, upon separating the overall displacements of the unit cell as a whole from that of the elements within it according to $\boldsymbol{r}_{j,\kappa}(t) = \boldsymbol{r} + \boldsymbol{r}_j + \boldsymbol{r}_\kappa + \boldsymbol{u}_j(t) + \boldsymbol{u}'_{j,\kappa}(t)$, the potential can be expanded in the global unit cell displacement $\{\boldsymbol{u}_j(t)\}$ only. This gives

$$V = \sum_{j,\kappa} v(\boldsymbol{r} - \boldsymbol{r}_j - \boldsymbol{r}_\kappa - \boldsymbol{u}'_{j,\kappa}) + \nabla_r \cdot \sum_{j,\kappa} v(\boldsymbol{r} - \boldsymbol{r}_j - \boldsymbol{r}_\kappa - \boldsymbol{u}'_{j,\kappa})\boldsymbol{u}_j + \cdots, \tag{13}$$

which may be convenient when one wishes to examine the internal distortions of the unit cell due to vibrations of the elements within it.

Taking account of the expansion of the interaction potential in (9) and the form of the scattering operator (8), the differential reflection coefficient (7) becomes

$$\frac{\mathrm{d}R}{\mathrm{d}\Omega_f\,\mathrm{d}E} = \frac{k_f k_{fz}}{(2\pi)^3 \hbar L^2} \sum_G \int_{-\infty}^{+\infty} \mathrm{d}t \int \mathrm{d}\boldsymbol{R} \int \mathrm{d}\boldsymbol{R}' \exp\{\mathrm{i}[(\boldsymbol{K}+\boldsymbol{G})\cdot(\boldsymbol{R}-\boldsymbol{R}') - Et/\hbar]\}$$
$$\times \left\langle\!\!\left\langle \left(n_i, \boldsymbol{k}_i \middle| \mathscr{T} \exp\left[(\mathrm{i}/\hbar) \int_{-\infty}^{+\infty} V^0(s)\,\mathrm{d}s + (i/\hbar) \int_{-\infty}^{+\infty} V^1(\alpha; s)\,\mathrm{d}s \right] \middle| \boldsymbol{k}_f \right) \right.\right.$$
$$\left.\left. \times \left(\boldsymbol{k}_f \middle| \mathscr{T} \exp\left[(-\mathrm{i}/\hbar) \int_{-\infty}^{+\infty} V^0(s')\,\mathrm{d}s' - (\mathrm{i}/\hbar) \int_{-\infty}^{+\infty} V^1(\alpha'; s')\,\mathrm{d}s' \right] \middle| \boldsymbol{k}_i, n_i \right) \right\rangle\!\!\right\rangle, \tag{14}$$

where the additional driving parameters are $\alpha = (\boldsymbol{R}, 0)$ and $\alpha' = (\boldsymbol{R}', t)$. In spite of the complicated appearance of eq. (14), the effect of the average over initial crystal states will be to produce an operator which is periodic with the symmetry of the static lattice. This means that in the matrix elements, the spatial integrals can be reduced to integrals over single unit cells, together with discrete summation over all unit cells. Using the expansion (12) for the interaction potential, the differential reflection coefficient then becomes

$$\frac{\mathrm{d}R}{\mathrm{d}\Omega_f\,\mathrm{d}E}$$
$$= \frac{k_f k_{fz}}{(2\pi)^3 \hbar L^2} \sum_G \int_{-\infty}^{+\infty} \mathrm{d}t \int \mathrm{d}\boldsymbol{R} \int \mathrm{d}\boldsymbol{R}' \exp\{\mathrm{i}[(\boldsymbol{K}+\boldsymbol{G})\cdot(\boldsymbol{R}-\boldsymbol{R}') - Et/\hbar]\} \sum_{l,l'} \exp[\mathrm{i}\boldsymbol{K}\cdot(\boldsymbol{R}_{l'} - \boldsymbol{R}_l)]$$
$$\times \left\langle\!\!\left\langle \left(n_i, \boldsymbol{k}_i \middle| \mathscr{T} \exp\left[(\mathrm{i}/\hbar) \int_{-\infty}^{+\infty} V^0(s)\,\mathrm{d}s + (\mathrm{i}/\hbar) \int_{-\infty}^{+\infty} \sum_{j,\kappa} \boldsymbol{f}_{j,\kappa} \cdot \boldsymbol{u}_{j+l,\kappa}(\alpha; s)\,\mathrm{d}s \right] \middle| \boldsymbol{k}_f \right)_{\text{u.c.}} \right.\right.$$
$$\left.\left. \left(\boldsymbol{k}_f \middle| \mathscr{T} \exp\left[(-\mathrm{i}/\hbar) \int_{-\infty}^{+\infty} V^0(s')\,\mathrm{d}s' - (\mathrm{i}/\hbar) \int_{-\infty}^{+\infty} \sum_{j',\kappa'} \boldsymbol{f}_{j',\kappa'} \cdot \boldsymbol{u}_{j'+l',\kappa'}(\alpha'; s')\,\mathrm{d}s' \right] \middle| \boldsymbol{k}_i, n_i \right)_{\text{u.c.}} \right\rangle\!\!\right\rangle. \tag{15}$$

In order to make further progress toward explicit calculations with (15) it is necessary to deal with the commutation of the various terms of the potential in the exponentials. A convenient way of treating this is through the trajectory approximation discussed above. The force is evaluated along a single classical trajectory of the potential V^0 characterized by the time-dependent path $\boldsymbol{r}(s)$ [25,42]. With the trajectory approximation the potential V^1 depends only on the crystal displacements, while because of its definition V^0 depends only on the particle coordinates, and the two terms commute. The differential reflection coefficient simplifies to

$$\begin{aligned}\frac{\mathrm{d}R}{\mathrm{d}\Omega_f\,\mathrm{d}E} = \frac{k_f k_{fz}}{(2\pi)^3\hbar L^2}\sum_{\boldsymbol{G}}\int_{-\infty}^{+\infty}\mathrm{d}t\int\mathrm{d}\boldsymbol{R}\int\mathrm{d}\boldsymbol{R}'\,\exp\{\mathrm{i}[(\boldsymbol{K}+\boldsymbol{G})\cdot(\boldsymbol{R}-\boldsymbol{R}')-Et/\hbar]\}\\ \times\sum_{l,l'}\exp[\mathrm{i}\boldsymbol{K}\cdot(\boldsymbol{R}_{l'}-\boldsymbol{R}_l)]\left|\left(\boldsymbol{k}_f\middle|\exp\left[(-\mathrm{i}/\hbar)\int_{-\infty}^{+\infty}V^0(s)\,\mathrm{d}s\right]\middle|\boldsymbol{k}_i\right)_{\mathrm{u.c.}}\right|^2\\ \times\left\langle\!\!\left\langle\exp\left[(\mathrm{i}/\hbar)\int_{-\infty}^{+\infty}\sum_{j,\kappa}\boldsymbol{f}_{j,\kappa}\cdot\boldsymbol{u}_{j+l,\kappa}(\alpha;s)\,\mathrm{d}s\right]\right.\right.\\ \left.\left.\times\exp\left[-(\mathrm{i}/\hbar)\int_{-\infty}^{+\infty}\sum_{j',\kappa'}\boldsymbol{f}_{j',\kappa'}\cdot\boldsymbol{u}_{j'+l',\kappa'}(\alpha';s')\,\mathrm{d}s'\right]\right\rangle\!\!\right\rangle,\end{aligned}\tag{16}$$

The thermal average in (16) can now be carried out. For operators linear in the harmonic displacements the commutations are handled with the relation $\exp(A)\exp(B)=\exp(A+B)\exp([A,B]/2)$, and $\langle\langle\exp(A)\rangle\rangle=\exp(\langle\langle A^2/2\rangle\rangle)$. The result is

$$\begin{aligned}\frac{\mathrm{d}R}{\mathrm{d}\Omega_f\,\mathrm{d}E} = \frac{\rho k_f k_{fz}}{(2\pi)^3\hbar L^2}\sum_{\boldsymbol{G}}\int_{-\infty}^{+\infty}\mathrm{d}t\int\mathrm{d}\boldsymbol{R}\int\mathrm{d}\boldsymbol{R}'\,\exp\{\mathrm{i}[(\boldsymbol{K}+\boldsymbol{G})\cdot(\boldsymbol{R}-\boldsymbol{R}')-Et/\hbar]\}\\ \times|\sigma_{fi}|^2\sum_l\exp(\mathrm{i}\boldsymbol{K}\cdot\boldsymbol{R}_l)\,\exp(-W(\boldsymbol{R},\boldsymbol{k}))\,\exp(-W(\boldsymbol{R}',\boldsymbol{k}))\,\exp(2\mathscr{W}_l(\boldsymbol{R},\boldsymbol{R}',t)),\end{aligned}\tag{17}$$

where the scattering amplitude is

$$\sigma_{fi}=\left(\boldsymbol{k}_f\middle|\exp\left[(-\mathrm{i}/\hbar)\int_{-\infty}^{+\infty}V^0(s)\,\mathrm{d}s\right]\middle|\boldsymbol{k}_i\right)_{\mathrm{u.c.}}.\tag{18}$$

The displacement correlation function depends only on the relative distance $l-l'$ between unit cells

$$\mathscr{W}_l(\boldsymbol{R},\boldsymbol{R}',\boldsymbol{r})=\frac{1}{\hbar^2}\left\langle\!\!\left\langle\int_{-\infty}^{+\infty}\sum_{j,\kappa}\boldsymbol{f}_{j,\kappa}\cdot\boldsymbol{u}_{j,\kappa}(\alpha;s)\,\mathrm{d}s\int_{-\infty}^{+\infty}\sum_{j',\kappa'}\boldsymbol{f}_{j',\kappa'}\cdot\boldsymbol{u}_{j'+l,\kappa'}(\alpha';s')\,\mathrm{d}s'\right\rangle\!\!\right\rangle\tag{19}$$

and the Debye–Waller exponent is $W(\boldsymbol{R},\boldsymbol{k})=\mathscr{W}_{l=0}(\boldsymbol{R},\boldsymbol{R},t=0)$.

Equation (17) is a quite general expression in which the only major approximations, aside from the harmonic approximation, are the expansion of the interaction potential through linear terms only and the application of the trajectory approximation. The $\boldsymbol{G}=\boldsymbol{0}$ term of (17) is essentially identical to the result presented by Bortolani and Levi [25] with two exceptions, we have accounted for the periodicity of the lattice which is recovered after averaging over the initial states of the crystal, and the scattering amplitude σ_{fi} does not depend on the variable $\boldsymbol{R}$. This latter difference is simply due to the choice of

separation of the interaction potential into the parts V^0 and V^1; making a different choice in which V^0 contains displacements of the basis elements which distort the unit cell such as in eq. (13), will lead to

$$|\sigma_{fi}|^2 = \sigma_{fi}^{\dagger}(\boldsymbol{R})\ \sigma_{fi}(\boldsymbol{R}') \tag{20}$$

after making a reasonable set of simplifying assumptions [65].

We note here that the spatial integrals over $\boldsymbol{R}$ and $\boldsymbol{R}'$ in the differential coefficient of (17) can be replaced by integrals over a single unit cell. Translation through a lattice vector such as in the operation $\boldsymbol{R} \to \boldsymbol{R} + \boldsymbol{R}_l$ simply changes the phase of the displacement vector. The correlation function (19) depends only on the phase difference, and this phase difference is summed over in (17). Thus the reduction of the spatial integrals to integrals over single unit cells merely multiplies (17) by a constant equal to the corresponding density of states.

General theories of inelastic surface scattering based on the powerful S-matrix formalism have been developed earlier by Brenig [49] and by Brako and Newns [42] and even much earlier by Beeby [38]. Equation (17) is more general than these earlier theories in two aspects, interference in multiphonon scattering arising from contributions from different surface unit cells is accounted for in the summation over lattice sites, and there is a multiplicative form factor $|\sigma_{fi}|^2$ which shows that the scattering from a single unit cell provides an envelope for the overall scattering distribution. For example, the theory of Brako and Newns in the form as developed by Celli and Himes [37,67] is recovered exactly if in eq. (17) only the term $l = 0$ and $\boldsymbol{G} = \boldsymbol{0}$ is retained and if $|\sigma_{fi}|^2$ is set equal to unity.

4. Quick scattering limit

We now come to the question of extraction the quick collision result out of the more general trajectory approximation of (17). For this we need to consider the phase generated by the trajectory approximation, for example as it appears in the correlation function of eq. (19):

$$\mathscr{S} = \frac{1}{\hbar}\int_{-\infty}^{+\infty} \sum_{j,\kappa} f_{j,\kappa}(\boldsymbol{r}(s)) \cdot \boldsymbol{u}_{j+l,\kappa}(\boldsymbol{R}, t; s)\ \mathrm{d}s, \tag{21}$$

and assuming that the collision is rapid compared to the important and dominant vibrational frequencies which will contribute to multiphonon processes, this becomes

$$\mathscr{S} \to \frac{1}{\hbar}\sum_{j,\kappa} \boldsymbol{u}_{j+l,\kappa}(\boldsymbol{R}, t) \cdot \int_{+\infty}^{-\infty} f_{j,\kappa}(\boldsymbol{r}(s))\ \mathrm{d}s = \sum_{j,\kappa} \boldsymbol{u}_{j+l,\kappa}(\boldsymbol{R}, t) \cdot \boldsymbol{k}_{j,\kappa}, \tag{22}$$

where $\hbar\boldsymbol{k}_{j,\kappa}$ is the momentum exchanged by a classical particle with the (l, κ) surface atom

$$\boldsymbol{k}_{j,\kappa} = \int_{-\infty}^{+\infty} f_{j,\kappa}(\boldsymbol{r}(s))\ \mathrm{d}s \tag{23}$$

The next and final assumption is that all atoms in the neighborhood of the classical point of collision have approximately the same phase and amplitude of displacement:

$$\mathscr{S} \to \boldsymbol{u}_l(\boldsymbol{R}, t) \cdot \sum_{j,\kappa} \boldsymbol{k}_{j,\kappa} = \boldsymbol{k} \cdot \boldsymbol{u}_l(\boldsymbol{R}, t). \tag{24}$$

The end result is to produce a correlation function (19) of the simple and well known form

$$\mathscr{W}_l(\boldsymbol{R}, \boldsymbol{R}', t) = \langle\langle (\boldsymbol{k} \cdot \boldsymbol{u}_0(\boldsymbol{R}, 0))(\boldsymbol{k} \cdot \boldsymbol{u}_l(\boldsymbol{R}', t))\rangle\rangle, \tag{25}$$

i.e., the time-dependent displacement correlation function.

Inserting the approximate form (25) into the differential reflection coefficient of (17) above gives

$$\frac{dR}{d\Omega_f\, dE} = \frac{\rho k_f k_{fz}}{(2\pi)^3 \hbar L^2} \sum_G \int_{-\infty}^{+\infty} dt \int_{u.c.} dR \int_{u.c.} dR'\, e^{i[(K+G)\cdot(R-R')-Et/\hbar]}$$

$$\times |\sigma_{fi}|^2 \sum_l e^{iK\cdot R_l}\, e^{-W(R,k)}\, e^{-W(R',k)}\, e^{\langle\langle(k\cdot u_0(R,0))(k\cdot u_l(R',t))\rangle\rangle}, \tag{26}$$

with the Debye–Waller exponent taking on the classic form $W(R, k) = \langle\langle |k\cdot u_l(R, t)|^2\rangle\rangle/2$.

At this point we have spelled out a complete set of approximations necessary to obtain the straightforward form of the differential reflection coefficient (26) in the quick collision limit. Before discussing the implications and applicability of the limit we would like to present a different route through which the identical result can be obtained. Rather than starting from the probability density (4) as was done in section 2, we can begin with the transition rate $w(k_f, k_i)$ for scattering from the initial state k_i to the final state k_f which is given by

$$w(k_f, k_i) = \frac{2\pi}{\hbar} \left\langle\!\!\left\langle \sum_{nf} |T_{fi}|^2 \delta(E_f - E_i) \right\rangle\!\!\right\rangle, \tag{27}$$

where E_g stands for the total energy of the system of projectile plus crystal. The transition rate is proportional to the time derivative of the probability density, and both contain the same information. The standard treatment is to use the interaction picture in which the time dependence of operators is driven by the crystal Hamiltonian [66]:

$$\hat{T}(t) = e^{iH^c t/\hbar} \hat{T}\, e^{-iH^c t/\hbar}. \tag{28}$$

If one now makes the following simple and straightforward approximation to the matrix elements of the transition operator taken with respect to particle eigenstates,

$$T_{k_f,k_i}(t) = \left(k_f \middle| \hat{T}(t) \middle| k_i\right) = \sum_{l,\kappa} e^{-ik\cdot[r_l + r_\kappa + u_{l,\kappa}(t)]} \tau^\kappa_{k_f,k_i}, \tag{29}$$

i.e., the only dependence on the crystal displacements is in the phase arising from the optical path, then the differential reflection coefficient resulting from (27) is

$$w(k_f, k_i) = \frac{1}{\hbar^2} \int_{-\infty}^{+\infty} dt\, e^{-iEt/\hbar} \sum_\kappa \sum_{\kappa'} \tau^\kappa_{fi} \left(\tau^{\kappa'}_{fi}\right)^* e^{-ik\cdot(r_\kappa - r_{\kappa'})}$$

$$\times \sum_l e^{iK\cdot R_l} \times e^{-W_\kappa(k)}\, e^{-W_{\kappa'}(k)}\, e^{\langle\langle(k\cdot u_{l',\kappa'}(0))(k\cdot u_{l,\kappa}(t))\rangle\rangle}. \tag{30}$$

This form of the transition rate is remarkably similar to the $G = 0$ term of eq. (26) above. In fact, if we take the limit in which the unit cell element divisions denoted by the index κ become small, and replace the summations over (κ, κ') by integrals over a single surface layer, the result is identical to the $G = 0$ term of (26) except that the scattering amplitude σ_{fi} takes on the (R, R') dependence discussed in eq. (20). The higher order terms in the reciprocal lattice vectors $G \neq 0$ appearing in (26) describe contributions from the diffraction components of the wave amplitude scattered by the elastic part of the perturbation potential. They become important only for highly diffractive systems. The final relation

between eqs. (26) and (30) lies in the relation between the scattering amplitudes τ_{fi} and σ_{fi}

$$|\tau_{fi}| = \frac{\hbar^2\sqrt{k_{fz}k_{iz}}}{L^3 m}|\sigma_{fi}|, \tag{31}$$

and the relation between the transition rate and the differential reflection coefficient

$$\frac{\mathrm{d}R}{\mathrm{d}\Omega_f\,\mathrm{d}E} = \frac{L^4}{(2\pi\hbar)^3}\frac{m^2 k_f}{k_{iz}} w(\boldsymbol{k}_f, \boldsymbol{k}_i). \tag{32}$$

The Debye–Waller factor is now given by the classic expression, whose exponent is the mean square displacement of a surface element

$$W_\kappa(\boldsymbol{k}) = \tfrac{1}{2}\langle\langle\, |\, \boldsymbol{k}\cdot\boldsymbol{u}_{,\kappa}(t)\,|^2\rangle\rangle. \tag{33}$$

This exercise has demonstrated that the quick collision approximation is completely equivalent to making the assumption of eq. (29) for the form of the transition matrix. This is similar to the type of assumptions that one makes for the scattering of neutrons or for X-rays. The derivation of a clear definition in (31) of the scattering amplitude τ_{fi} from the trajectory approximation (18) shows that the neutron-like scattering assumption of (29) can indeed be applied to atom–surface scattering in the case of multiple quantum exchanges, when the modes involved are low frequency and long wavelength. Normally such an approximation is not considered valid for systems in which there is multiple scattering beween different scattering centers. However, in the atom–surface case, in spite of its strong and multiple scattering nature, such an assumption again becomes useful because of the two-dimensional character of the scattering zone. However, there are clear limitations to such an assumption. For example, it is not expected to give a complete description of single surface phonon exchange except possibly in the long wavelength acoustic limit, and it is not valid when the wave packet of the probe has components which reside for long times near the surface such as in selective adsorption resonances.

At this point we have clearly derived a complete set of approximations necessary to obtain the rather simple form of the inelastic scattering intensity in the quick collision limit. The approximations applied to the trajectory approximation limit are made explicit in eqs. (21)–(25), and show that only small frequency and long wavelength phonon modes are considered, and optical modes enter only as a possible temperature and position dependence of the scattering amplitude as in (20). The lowest-order approximation to the scattering amplitude τ_{fi} is clearly identified in eq. (18) as the off-energy-shell transition matrix element of the elastic part of the interaction potential. Although τ_{fi} (or alternatively σ_{fi}) is a matrix element taken only over a single unit cell, it includes multiple scattering with all neighboring unit cells which can occur via the first order interaction potential V^0.

From the calculational point of view, this justification is important because of the great simplicity afforded by the multiphonon scattering intensity of eq. (26) or (30) as opposed to the full trajectory approximation of eq. (17), and this advantage becomes particularly pronounced when the quick collision approximation is used with simple models for the vibrational displacements such as Debye or Einstein models. The success of this simpler approach in explaining the multiphonon intensities for numerous systems ranging from the quantum mechanical regime [68–70] to nearly classical scattering [71], some of which are presented in Section 8 below, shows that these assumptions have a broad range of applicability.

Finally, it is noted that the reduction of the full trajectory approximation of eq. (17) to the fast collision approximation of (26) or (30) provides, in the intervening steps, a hierarchy of different stages of approximation which may prove to be useful in special cases.

5. Phonon expansion

We now exhibit the scattered intensity as an ordered series in terms of the number of phonons exchanged between the projectile and the crystal. We take the transition rate of eq. (30) as the starting point, and the multiphonon series is obtained by expanding the exponential of the correlation function:

$$e^{\langle\langle(\boldsymbol{k}\cdot\boldsymbol{u}_{l',\kappa'}(0))(\boldsymbol{k}\cdot\boldsymbol{u}_{l,\kappa}(t))\rangle\rangle} = 1 + \langle\langle(\boldsymbol{k}\cdot\boldsymbol{u}_{l',\kappa'}(0))(\boldsymbol{k}\cdot\boldsymbol{u}_{l,\kappa}(t))\rangle\rangle + \tfrac{1}{2}\langle\langle(\boldsymbol{k}\cdot\boldsymbol{u}_{l',\kappa'}(0))(\boldsymbol{k}\cdot\boldsymbol{u}_{l,\kappa}(t))\rangle\rangle^2 + \cdots . \tag{34}$$

When (34) is inserted back into (30), this leads to a transition rate which is a corresponding series of terms

$$w(\boldsymbol{k}_f, \boldsymbol{k}_i) = w^{(0)}(\boldsymbol{k}_f, \boldsymbol{k}_i) + w^{(1)}(\boldsymbol{k}_f, \boldsymbol{k}_i) + w^{(2)}(\boldsymbol{k}_f, \boldsymbol{k}_i) + \cdots , \tag{35}$$

where the superscripts on the right hand side indicate the number of exchanged phonons.

The elastic, or zero quantum exchange term can be immediately written down:

$$w^{(0)}(\boldsymbol{k}_f, \boldsymbol{k}_i) = \frac{2\pi}{\hbar}\sum_G \left|\sum_\kappa \tau_{fi}^\kappa\, e^{-W_\kappa(k)}\, e^{-i\boldsymbol{k}\cdot\boldsymbol{r}_\kappa}\right|^2 \delta_{G,K}\delta(E). \tag{36}$$

The delta functions show that the elastic scattering intensity is non-vanishing only when the conditions of conservation of energy and momentum parallel to the surface are satisfied. If the unit cell is a Bravais cell and we consider scattering from only the outer surface layer, then the elastic transition rate reduces to

$$w^{(0)}(\boldsymbol{k}_f, \boldsymbol{k}_i) = \frac{2\pi}{\hbar}\sum_G |\tau_{fi}|^2\, e^{-2W(k)}\delta_{G,K}\delta(E). \tag{37}$$

This is in a very standard form. It is the product of a form factor $|\tau_{fi}|^2$ for scattering from a single unit cell, multiplied by a Debye–Waller factor $e^{-2W(k)}$ and a structure factor expressed by the δ-functions.

The single phonon exchange is the first-order term in the expansion of (35) and is

$$w^{(1)}(\boldsymbol{k}_f, \boldsymbol{k}_i) = \frac{1}{\hbar^2}\int_{-\infty}^{+\infty} dt\, e^{-iEt/\hbar}\sum_\kappa\sum_{\kappa'}\tau_{fi}^\kappa(\tau_{fi}^{\kappa'})^*\, e^{-i\boldsymbol{k}\cdot(\boldsymbol{r}_\kappa-\boldsymbol{r}_{\kappa'})} \times\sum_l e^{i\boldsymbol{K}\cdot\boldsymbol{R}_l}\, e^{-W_\kappa(k)}\, e^{-W_{\kappa'}(k)}\langle\langle(\boldsymbol{k}\cdot\boldsymbol{u}_{0,\kappa'}(0))(\boldsymbol{k}\cdot\boldsymbol{u}_{l,\kappa}(t))\rangle\rangle. \tag{38}$$

The displacement correlation function can be evaluated explicitly in the case of a lattice in the harmonic approximation. The αth Cartesian component of the surface atomic displacement operator can be expanded in the normal harmonic modes of the crystal,

$$u_{l,\kappa}^\alpha(t) = \sum_{Q,\nu}\sqrt{\frac{\hbar}{2NM_\kappa\omega_\nu(Q)}}\, e_\alpha\left(\kappa\middle|\frac{Q}{\nu}\right)e^{iQ\cdot(R_l+R_\kappa)} \times\left[a_\nu^\dagger(Q)\, e^{-i\omega_\nu(Q)t} + a_\nu(-Q)\, e^{i\omega_\nu(Q)t}\right], \tag{39}$$

where M_κ is the mass of the κth surface atom, Q is the parallel wave vector of the mode, ν is a discrete quantum number for surface modes and continuous for bulk modes; $e_\alpha(\kappa|\frac{Q}{\nu})$ is the polarization vector of the (Q, ν) mode, $\omega_\nu(Q)$ is the mode frequency, and $a_\nu^\dagger(Q)$ is the creation operator. The sum over Q is limited to a single surface Brillouin zone.

The displacement correlation function now becomes

$$\langle\langle (\boldsymbol{k}\cdot\boldsymbol{u}_{l',\kappa'}(0))(\boldsymbol{k}\cdot\boldsymbol{u}_{l,\kappa}(t))\rangle\rangle = \sum_{\alpha,\alpha'=1}^{3} k_\alpha k_{\alpha'} \sum_{Q,\nu} \frac{\hbar}{2N\sqrt{M_\kappa M_{\kappa'}}\,\omega_\nu(Q)} \times e_\alpha\left(\kappa\middle|\frac{Q}{\nu}\right) e^*_{\alpha'}\left(\kappa'\middle|\frac{Q}{\nu}\right) e^{iQ\cdot(R_{l,\kappa}-R_{l',\kappa'})} \times\{[2n(\omega_\nu(Q))+1]\cos(\omega_\nu(Q)t) - i\sin(\omega_\nu(Q)t)\}, \tag{40}$$

where $n(\omega_\nu(Q))$ is the Bose–Einstein function

$$n(\omega_\nu(Q)) = [e^{\hbar\omega_\nu(Q)/k_B T} - 1]^{-1}, \tag{41}$$

with T the temperature of the surface and k_B Boltzmann's constant.

Combining (38) with (40) and carrying out the straightforward summations, we obtain the final result for the single phonon transition rate:

$$w^{(1)}(\boldsymbol{k}_f, \boldsymbol{k}_i) = \frac{2\pi\rho S_{\text{u.c.}}}{\hbar} \sum_{\alpha,\alpha'=1}^{3} k_\alpha k_{\alpha'} \sum_{\kappa,\kappa'} \tau^\kappa_{fi}(\tau^{\kappa'}_{fi})^*\, e^{-W_\kappa(k)}\, e^{-W_{\kappa'}(k)}\, e^{-ik_z(z_\kappa - z_{\kappa'})} \times [\rho^{\alpha,\alpha'}_{\kappa,\kappa'}(-K, E)[n(E/\hbar)+1] + \rho^{\alpha,\alpha'}_{\kappa,\kappa'}(K, E)\, n(E/\hbar)]. \tag{42}$$

This is written in terms of the phonon spectral density, essentially the Fourier transform of the displacement correlation function evaluated at zero temperature, which is defined by

$$\rho^{\alpha,\alpha'}_{\kappa,\kappa'}(K, E) = \sum_\nu \frac{\hbar}{2S_{\text{u.c.}}\sqrt{M_\kappa M_{\kappa'}}\,\omega_\nu(K)} \times e_\alpha\left(\kappa\middle|\frac{Q}{\nu}\right) e^*_{\alpha'}\left(\kappa'\middle|\frac{Q}{\nu}\right) \delta(E/\hbar - \omega_\nu(K)). \tag{43}$$

Equations (42) and (43) show that for the exchange of discrete surface modes (e.g., Rayleigh modes, and other modes for which the energy is completely specified by the parallel momentum) the intensity appears as a sharp peak in an energy resolved measurement. The term proportional to $n(E/\hbar)+1$ is for phonon creation and the term proportional to $n(E/\hbar)$ is for phonon annihilation.

Now that the forms of the elastic and single phonon contributions have been established, it is straightforward to obtain the multiphonon contribution, which is clearly given by all terms of order 2 and greater in eq. (35). In practice eq. (30), after subtracting off the elastic and single quantum contributions, can be used as a starting point for a completely numerical calculation of the multiphonon scattering. The time-dependent displacement correlation function (40) can be evaluated using any standard calculational methods for surface vibrations, e.g., a slab calculation or Green-functions methods. The Fourier transform over time in (30) is well behaved and can be carried out, and the sum over lattice positions converges rapidly, as we show in the next section below.

It is of interest to emphasize that, within the quick collision approximation used here, the form factor for the single phonon intensity is identical to that for multiple phonon scattering. This implies that measurements of both the single phonon intensity and the multiphonon background provide sufficient information to unambiguously determine both the form factor and the spectral density independently. Measurements of the single phonon intensity alone are not sufficient for this, since the form factor is always multiplied by the spectral density, and only the product of the two can be determined by measurement.

6. First-order semiclassical limit

In keeping with the assumption that only long wavelength and small frequency phonons contribute strongly to the multiphonon part of the inelastic intensity, a further important simplification is possible. This consists of making an expansion in small wave vectors on the term $\exp\{i\boldsymbol{Q}\cdot(\boldsymbol{R}_{l,\kappa}-\boldsymbol{R}_{l',\kappa'})\}$ appearing in the displacement correlation function of (40). Simplifying to the case of a Bravais surface unit cell, and including terms through third order in $\boldsymbol{Q}\cdot\boldsymbol{R}_l$, leads to a form for the transition rate of eq. (30) which is expressed quite simply as

$$w(\boldsymbol{k}_f,\boldsymbol{k}_i)=\frac{\rho}{\hbar^2}|\tau_{fi}|^2\,\mathrm{e}^{-2W(k)}S(\boldsymbol{K},E)\;I(\boldsymbol{K},E), \tag{44}$$

where

$$S(\boldsymbol{K},E)=\sum_l \mathrm{e}^{-i\boldsymbol{K}\cdot\boldsymbol{R}_l}\,\mathrm{e}^{-F_l}, \tag{45}$$

with

$$F_l=\sum_{\alpha,\alpha'=1}^{3}k_\alpha k_{\alpha'}\sum_{Q,\nu}\frac{\hbar(\boldsymbol{Q}\cdot\boldsymbol{R}_l)^2}{2NM\omega_\nu(\boldsymbol{Q})}e_\alpha\binom{Q}{\nu}\,e^*_{\alpha'}\binom{Q}{\nu}\left[2n(\omega_\nu(\boldsymbol{Q}))+1\right], \tag{46}$$

and

$$I(\boldsymbol{K},E)=\int_{-\infty}^{+\infty}\mathrm{d}t\;\mathrm{e}^{-iEt/\hbar}\,\mathrm{e}^{Q(t)}, \tag{47}$$

with

$$Q(t)=\sum_{\alpha,\alpha'=1}^{3}k_\alpha k_{\alpha'}\sum_{Q,\nu}\frac{\hbar}{2NM\omega_\nu(\boldsymbol{Q})}e_\alpha\binom{Q}{\nu}\,e_{\alpha'}\binom{Q}{\nu}$$
$$\times\left(\left[2n(\omega_\nu(\boldsymbol{Q}))+1\right]\cos(\omega_\nu(\boldsymbol{Q})t)-i\sin(\omega_\nu(\boldsymbol{Q})t)\right). \tag{48}$$

In the limit $t\to 0$, $Q(t)$ is just the Debye–Waller exponent of eq. (33), and F_l is a closely related sum in which the summand is weighted by the square of the parallel momentum.

The transition rate of eq. (44) is the product of a form factor $|\tau_{fi}|^2$, a Debye–Waller factor, a structure factor $S(\boldsymbol{K},E)$ arising from the periodic distribution of surface atoms, and an energy exchange factor $I(\boldsymbol{K},E)$. At high temperatures and large momentum transfers the structure factor is a rapidly convergent sum over lattice sites, since eq. (46) shows that F_l varies as $\boldsymbol{R}_l^2$.

At higher temperatures and momentum exchange, a further expansion in small times can be made on the imaginary part of $Q(t)$ which leads to $\mathrm{Im}\;Q(t)=-i\omega_0 t$, with

$$\omega_0=\frac{\hbar k^2}{2M}. \tag{49}$$

The $\mathrm{Im}\;Q(t)$ is simply an energy shift appearing in the Fourier transform of the energy transfer function (47) which has its origins in the zero-point motion of the lattice. It is interesting that even though the zero-point motion is usually considered a low temperature effect, here it has an important manifestation in the semiclassical limit of high temperature and incident energy. In the "true semiclassical" limit in which the incident and final energies must be large and very nearly the same, $\hbar\omega_0$ is readily shown to be

the average energy given up to the surface by the incident projectile. The importance of zero-point motion in this context is noted even in the case of high energy ion scattering [51,72,73].

It is of interest to discuss the form of the structure factor $S(\boldsymbol{K}, E)$ appearing in (45). It has the appearance of a structure factor for elastic diffraction, but the summand is weighted by a Gaussian damping function in $\boldsymbol{R}_l$ which depends on T and momentum exchange $\boldsymbol{k}$. It is peaked at values of $\boldsymbol{K}$ equal to the reciprocal lattice vectors $\boldsymbol{G}$, and near these positions can be approximated by a Gaussian function in $\boldsymbol{K}$. For non-simple surface unit cells, such as that of the fcc (111) surface, $S(\boldsymbol{K}, E)$ may exhibit additional structure between the diffraction peak positions. This behavior indicates that the multiphonon intensity may exhibit structure which can be associated with the diffraction peak positions. This structure is due to the coherent interference of the multiphonon amplitude scattered from neighboring unit cells.

In the classical limit of high T and large k, $S(\boldsymbol{K}, E) \to 1$ for a discrete lattice, since only a single term in the summation over lattice sites contributes. This behavior is quite physical and implies that the coherent region of the crystal surface which contributes to the multiphonon signal shrinks as one approaches classical conditions, and in the classical limit the coherence area shrinks to the interaction with a single surface atom. Thus, in the extreme semiclassical limit, the structure factor for scattering from a perfectly ordered surface is no different from the constant structure factor associated with an isolated defect, and the only difference between the coherent and the incoherent multiphonon intensity distribution for the two cases will be due to the difference in form factor.

7. Classical limit

The classical limit occurs for high temperatures and large energies (or more precisely, large k). Under classical scattering conditions the Debye–Waller factor is so small that elastic and single phonon peaks are completely suppressed, and only multiple phonon exchanges occur. There have been several recent and interesting treatments of semiclassical and classical trajectory approximations to the multiphonon scattering of atomic and molecular particles at surfaces which have considered the classical limit [37,43,49,51,52]. It is of interest to consider the present theory in this limit as it leads to closed form expressions for the scattering intensities, and gives specific criteria for the validity of the classical limit.

For scattering of a point projectile with a lattice of discrete atomic centers, we have already shown in section 6 above that the structure factor (45) is unity, signifying pairwise collisions with the lattice atoms. The energy exchange factor (47) is evaluated by the method of steepest descents, upon expanding $Q(t)$ of eq. (48) to order t^2. The final result is the following differential reflection coefficient:

$$\frac{\mathrm{d}R}{\mathrm{d}\Omega_f\,\mathrm{d}E} = \frac{m^2|k_f|}{8\pi^3\hbar^5 k_{iz}}|\tau_{fi}|^2\left(\frac{\hbar\pi}{\omega_0 k_B T}\right)^{1/2}\exp\left\{-\frac{(E+\hbar\omega_0)^2}{4k_B T\hbar\omega_0}\right\}. \tag{50}$$

The Debye–Waller factor no longer appears explicitly in this expression because it has been canceled by a term arising from the energy exchange factor. The scattering intensity is a Gaussian-like function in the energy exchange E, but shifted to the energy loss side by the energy shift $\hbar\omega_0$ of eq. (49). However, we note that this function is not a true Gaussian because ω_0 is a function of k. The intensity is limited on the energy loss side by the fact that the projectile may loose no more energy than it had initially, and it is skewed towards the energy gain side by the energy dependence of ω_0. The width of the differential reflection coefficient in energy exchange is roughly $2\sqrt{k_B T\hbar\omega_0}$ in energy units, and the peak amplitude decays with increasing temperature as $(k_B T\hbar\omega_0)^{1/2}$. This behavior of the width and peak intensity of the differential reflection coefficient is understandable in terms of the unitarity condition, which guarantees the equality of the number of scattered particles to the number of incident particles. At higher

temperatures the intensity spreads over a larger range of E, consequently in order to preserve the number of particles, the peak intensity must decrease accordingly.

The steepest descent evaluation of eq. (50) also implies a criterion for the validity of the semiclassical result which is

$$2W(k)/6 \gg 1. \tag{51}$$

This is a very stringent criterion, and is in fact rarely satisfied in typical He-scattering experiments, and often not satisfied even when the projectile is a heavier atom such as Ne or Ar. The average number of phonons exchanged in a collision process is approximately equal to $2W$, thus (51) implies that for the classical approximation to be valid, a truly large number of quanta must be exchanged. In practice it is found that for $2W < 6$ the differential reflection coefficient differs strongly from Gaussian form and is an increasing, rather than decreasing, function of T. For values of $2W \geq 6$ the Gaussian-like form of eq. (50) is a reasonable approximation.

Equation (50) is the classical limit for a point particle scattering from a lattice of scattering centers in the limit in which the projectile scatters from a single surface atom. There is a second classical limit for the case of an incident projectile which interacts with many surface atoms, and the surface can be treated as a continuum. This is the limit that should be applicable in the completely classical case of a projectile that is large compared to the inter atomic lattice spacing. In this limit, the structure factor (45) does not approach a constant, rather it has a Gaussian behavior in parallel momentum. This expression is obtained by replacing the summation over lattice sites in (45) by an integral. The final result is a differential reflection coefficient of the following form:

$$\frac{\mathrm{d}R}{\mathrm{d}\Omega_f\,\mathrm{d}E} = \frac{m^2|k_f|}{4\pi^3\hbar^5 k_{iz} S_{u.c.}} |\tau_{fi}|^2 v_R^2 \left(\frac{\hbar\pi}{\omega_0 k_B T}\right)^{3/2} \exp\left\{-\frac{(E+\hbar\omega_0)^2 + 2\hbar^2 v_R^2 K^2}{4k_B T\hbar\omega_0}\right\}, \tag{52}$$

where v_R is a characteristic velocity, or weighted average of surface phonon velocities parallel to the surface. There is a clear difference between the two classical limits (50) and (52). In the latter, the temperature dependence of the peak in the inelastic intensity varies as $1/T^{3/2}$ as opposed to $1/T^{1/2}$, and there is the extra Gaussian behavior in parallel momentum exchange.

Equation (52) with the form factor $|\tau_{fi}|^2$ taken to be constant is essentially the expression developed by Brako and Newns [43] and can be arrived at by purely classical thermodynamical treatments of scattering from an isotropic continuum surface [48]. The present treatment produces a specific expression for the energy shift ω_0 given by (49), whereas in a classical or semiclassical treatments [43,48] it is often chosen to be the Baule expression derived from binary particle collisions, modified by the presence of the attractive well,

$$\hbar\omega_0 \approx \frac{4\mu}{(1+\mu)^2}\left(E_i \cos^2(\theta_i) + D\right), \tag{53}$$

where $\mu = m/M$ is the ratio of the projectile to surface atom mass, E_i is the incident energy, and D is the depth of the attractive potential well in front of the surface. Equation (49), evaluated in the semiclassical limit where $k_{fz} \approx k_{iz}$ and $k \approx 2k_{iz}$, is very close to (53), namely

$$\hbar\omega_0 \approx \frac{4\hbar^2 k_{iz}^2}{2M} = 4\mu E_i \cos^2(\theta_i), \tag{54}$$

differing from the Baule expression only in the absence in the denominator of the factor $(1+\mu)^2$. We could readily include the well depth D in our treatment by using the same arguments inherent in (53), that the attractive part of the particle surface potential is rigid (and consequently does not contribute to

inelastic exchange) and is sufficiently smoothly varying that it also does not elastically backscatter an appreciable fraction of the incident particle amplitude [74–76].

An interesting special application of the classical limit is the case of the approach to an equilibrium distribution of a scattered gas arising from a very low energy beam of atoms incident on a very hot surface [65]. In the limit $E_i \ll E_f$ we have for the energy exchange and energy shift

$$E = E_f - E_i \to E_f \tag{55}$$

and

$$\hbar\omega_0 = \frac{\hbar^2}{2M}(\boldsymbol{k}_f - \boldsymbol{k}_i)^2 \to \frac{m}{M}E_f. \tag{56}$$

The differential reflection coefficient of eq. (52) then takes the form

$$\frac{\mathrm{d}R}{\mathrm{d}\Omega_f\,\mathrm{d}E} \propto T^{-3/2}\exp\left\{\frac{-E_f(1+m/M)^2}{4k_\mathrm{B}Tm/M}\right\}. \tag{57}$$

Due to the momentum dependence of the energy shift $\hbar\omega_0$, the Gaussian-like function of the energy exchange is skewed to the point where it becomes an exponential in the final energy of the scattered particle. This can be related to the final energy $\mathscr{E}$ of a crystal atom through the well known expression for the energy exchanged in a two particle collision

$$E_f = 4\mathscr{E}\frac{m/M}{(1+m/M)^2}, \tag{58}$$

leaving the scattered intensity in the form

$$\frac{\mathrm{d}R}{\mathrm{d}\Omega_f\,\mathrm{d}E} \propto T^{-3/2}\,\mathrm{e}^{-\mathscr{E}/k_\mathrm{B}T}. \tag{59}$$

The differential reflection coefficients of (59) or (57) clearly indicate not only that the incident low energy beam of particles has gained energy in the surface collision, but in addition show that the particles leave the surface with an energy distribution having the exponential dependence of the Maxwell–Boltzmann distribution function.

8. Comparisons with experiment

Experiments on He scattering by crystal surfaces provide many pertinent examples of the application of the multiphonon theory developed in this review. Typical experiments use He energies in the thermal range of 5–100 meV, where the de Broglie wavelength is of the order 0.1–1 Å, and hence the motion of the He projectiles is quantum mechanical. With surface temperatures ranging from T less than the surface Debye temperature Θ_D to several times Θ_D, the inelastic background is characterized by an average number of exchanged quanta $2W(\boldsymbol{k})$ which ranges from less than unity (the quantum regime) to values of 10 or greater (which, according to eq. (51) is well into the classical regime).

As examples we choose the three widely disparate systems of He scattered by alkali halide insulators, by close packed metal surfaces, and a surface consisting of a Langmuir–Blodgett film of long organic molecules. The highly corrugated alkali halides are strong inelastic scatterers, while the close packed metals are weak inelastic scatterers due to their flat and softer repulsive potential. The Langmuir–Blod-

gett film provides an example of a very soft surface in which the scattering distribution appears quite classical in spite of the quantum mechanical nature of the He projectile.

In order to make quantitative comparisons with experiment, the scattering amplitude τ_{fi}, or more precisely the form factor $|\tau_{fi}|^2$ must be specified. This has been studied in previous work explaining the intensities of single phonon inelastic peaks. Harten et al. [77] have found, through a careful consideration of pairwise summation potentials for the He–surface interaction potential V, that $|\tau_{fi}|^2$ can be expressed as the product of a cutoff function in parallel momentum $\boldsymbol{K}$ and the Mott–Jackson matrix element [78] in the perpendicular momentum:

$$|\tau_{fi}|^2 = \mathrm{e}^{-2K^2/Q_c^2} v_{\mathrm{M-J}}^2(k_{fz}, k_{iz}). \tag{60}$$

The Mott–Jackson factor $v_{\mathrm{M-J}}$ is the matrix element of the one-dimensional potential $v(z) = \exp(-\beta z)$ taken with respect to its own distorted eigenstates. The form factor (60) has exponential decay in K^2, and the Mott–Jackson factor behaves roughly as an exponential decay in the normal momentum difference $|k_{fz}| - |k_{iz}|$. The two parameters Q_c and β are best known for metal surfaces where it is found that the cutoff momentum Q_c is around 1 Å^{-1}, while the range parameter β is usually somewhat larger than 2 Å^{-1}.

Skofronick et al. [69,70] have recently carried out extensive investigations of both single phonon and multiphonon scattering of He by alkali halides. Figure 1 shows several energy resolved scans of the scattering of a 44 meV He beam from a NaCl (001) surface in the ⟨100⟩ azimuthal direction at different surface temperatures. The experiment is a so-called "specular" scan configuration in which $\theta_i = \theta_f$ and in this case θ_i is 45°. The solid curves in fig. 1 are the theoretical results given by the first order semiclassical differential reflection coefficient of eq. (44) using the form factor of (60). A Debye model is used for the phonons with a Debye temperature Θ_D of 224 K. The cutoff parameter is $Q_c = 5.6$ Å^{-1} and the range parameter is $\beta = 6$ Å^{-1}, both of which imply a very weak dependence of the form factor on the energy and momentum exchange. The value of v_R is unimportant, as the structure factor $S(\boldsymbol{K}, E)$ is essentially unity even for temperatures of order Θ_D.

The agreement between theory and experiment is good, and this agreement extends to all temperatures measured, from $T \simeq 100$ to 800 K. There is a small increase in the overall multiphonon intensity with T, and a nearly linear increase with T of the full width at half maximum. Both of these behaviors agree well with the calculations. Note that the classical result for the intensity (50) would predict a decrease in the maximum height of the inelastic intensity with T, in disagreement with experiment. For the higher temperatures the value of the Debye–Waller exponent is larger than unity (having a value of 4 for $T = 623$ K, implying about 4 real phonons exchanged per collision), and the energy shift $\hbar\omega_0$ is about 10 meV. This energy shift, although arising from zero-point motion, is clearly non-negligible; without it the experimental and calculated curves cannot be made to agree regardless of how the parameters are varied.

A further example of the He/NaCl(001) system is shown in Fig. 2. In this case the surface is in the ⟨110⟩ azimuthal direction and the beam is incident at the much lower energy of 28 meV. The surface temperature is 773 K. The inelastic background is strongly shifted to the energy gain side, and the agreement with calculations is again good. Values of $2W$ and $\hbar\omega_0$ at zero energy transfer are about 3 and 6 meV, respectively. This example is interesting because it a case of "cold" particles colliding with a "hot" surface in which particles on average gain energy.

Additional calculations of the total inelastic background for the same system as in fig. 2 at both higher and lower temperatures are shown in fig. 3. The highest temperature calculation exhibited is for $T = 1000$ K, and compared to the curve for $T = 773$ K, shows a broader width in the energy exchange and a decreased maximum amplitude. The decrease of the maximum amplitude at higher temperatures is characteristic of the classical limit of eq. (50), and at this temperature the system is just entering the

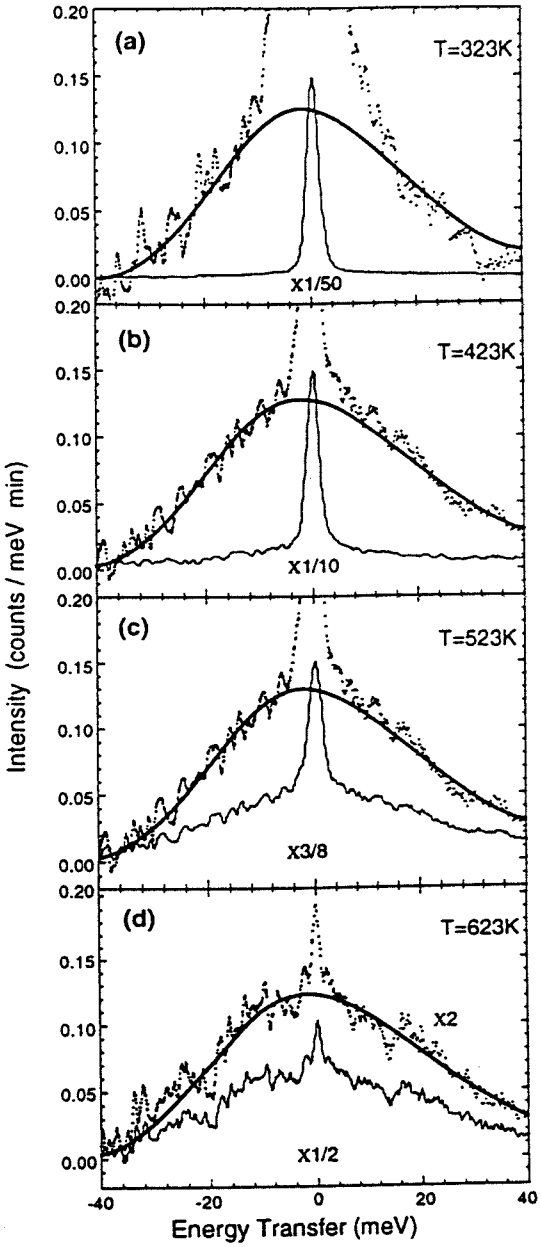

Fig. 1. Scattered intensity versus energy exchange for an incident beam of 44 meV He atoms incident on a clean NaCl(001) surface in the ⟨100⟩ direction for several surface temperatures. The incident and detector angles are both 45°. The vertical scales are for the dotted curves, which are the data expanded to show the inelastic foot. The light solid line is the data reduced to show the relative size of the elastic peak to the inelastic foot. The heavy solid lines are the theoretical calculations.

classical regime. The low temperature calculations in fig. 3 are for $T = 100$ K and show the characteristic oscillations that arise in the multiphonon background from the structure factor in eq. (45). For the $T = 100$ K curve, the multiple phonon contribution has been drawn in as a dashed line, in addition to the total inelastic background which includes the single quantum part. The single phonon part is the largest

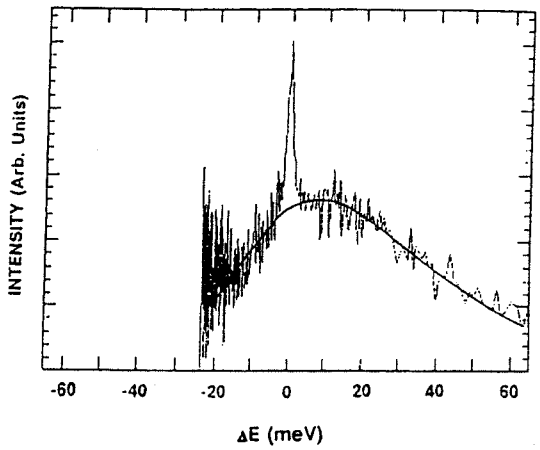

Fig. 2. Scattered intensity as a function of energy exchange for a beam of He incident on a NaCl(001) surface in the ⟨110⟩ direction. The incident energy is 28 meV, the surface temperature is 773 K, and the incident and detector angles are both 45°. The solid curve is the calculation.

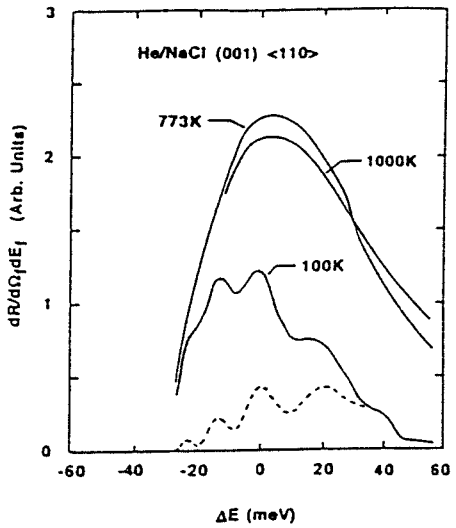

Fig. 3. Calculated differential reflection coefficients for the system of fig. 2 for three different surface temperatures: 773, 1000, and 100 K. For the 100 K calculation the solid line is the total inelastic intensity and the dashed curve is the multiphonon contribution.

contributor at this low temperature, but in the Debye approximation it is a relatively smoothly varying contribution, the structure appears entirely in the exchange of larger numbers of phonons. It is clear that the majority of the energy exchanged by the particle is through the single phonon term, and that net energy will be lost to the surface by the particles, contrary to the situation at higher temperatures.

Figure 4 shows an energy resolved specular scan of the scattering of a 37 meV incident beam of He on an Al(111) surface in the ⟨112⟩ direction, with the crystal temperature at 500 K. The solid curve shows the agreement with the calculations that is obtained using $Q_c = 1.3$ Å^{-1} and $\beta = 2.5$ Å^{-1} and a Debye temperature of 333 K. The value of v_R is unimportant as the structure factor is essentially unity. This

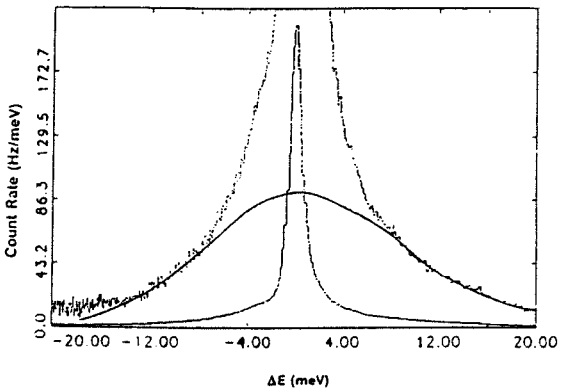

Fig. 4. Similar plot to figs. 1 and 2, except for an Al(111) surface in the ⟨112⟩ direction, incident energy 37 meV, and surface temperature of 500 K.

example shows that the nature of the multiphonon background from metal surfaces is radically different from that of the alkali halides. In figs. 1 and 2 the inelastic background formed pronounced and broad shoulders on which the specular intensity could be seen as a distinct, narrow spike. For metal surfaces the inelastic background is substantially weaker in intensity at all energies, and does not form distinct shoulders under the specular peak. This difference between insulators and metals is explained by the energy and momentum dependence of the form factor. The values of Q_c and β for Al (both choices being in agreement with typical values known for a wide range of metal surfaces [29]) imply a form factor correction as a function of energy exchange that is substantially stronger than that used for the alkali halide surfaces. These observations lead to two important conclusions: (i) the form factor of scattering by the unit cell can play a dominant role in the shape of the multiphonon background because of its strong dependence on the momentum transfer, and (ii) the strong dependence of the form factor on k is particularly pronounced in metals, because the potential is flat (implying small Q_c) and soft (small β), and these facts explains why the inelastic background from metals is weak and rapidly decaying as a function of energy exchange.

As a final example of the application of the theory developed here we consider He scattering from the surface of a Langmuir–Blodgett film and this provides an excellent example of the classical limit expression developed in section 7. Langmuir–Blodgett films consist of long organic molecules attached at one end to a substrate, and organized in an ordered array perpendicularly (or nearly so) to the substrate. The data shown in fig. 5 is for He scattering from a monolayer film of arachidic acid and methyl sterate (AAMS, in the molar ratio 9:1) [79,80]. The He energy is 30 meV, the mica substrate temperature is approximately 130 K, and it is a specular scan with incidence at $\theta_i = 60°$. Also shown in fig. 5 is the profile of the incident beam, including all broadening by the instrument. The complete absence of any sharp features in the intensity versus energy exchange plot indicates that the Debye–Waller factor is very small, and that the elastic and single phonon features are too weak to be observed. All of the scattered intensity is due to multiphonon inelastic exchanges, which implies that the classical expressions developed in section 7 should be applicable. The solid curve drawn in fig. 5 is the result of calculations using eq. (50) with a film temperature of 130 K as given by experiment and with an effective mass of $M = 15$ amu, which implies that the He atoms scatter from the methyl group of mass 15 which is the terminal group of the AAMS film. The form factor is chosen to be the semiclassical limit of the Mott–Jackson matrix element (60), $\tau_{fi} = 2\hbar^2 k_{fz} k_{iz}/m$.

The fit gives some interesting information. The Debye–Waller exponent evaluated at $E \approx 0$ has a value $2W \approx 15$, which places the experiment substantially beyond the classical condition of eq. (51) and

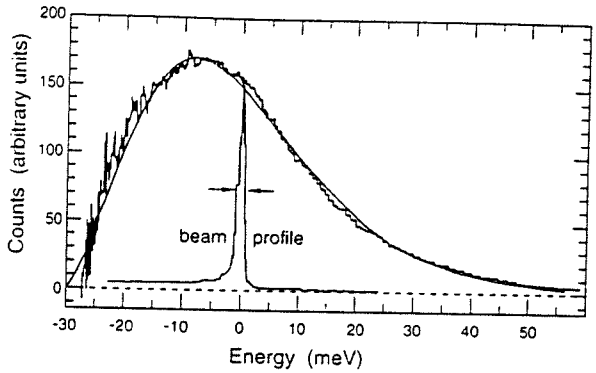

Fig. 5. The time-of-flight spectrum (histogram-like curve) converted to energy gain and loss for a monoenergetic He atom beam of energy 30 meV scattered from an AAMS monolayer surface at a temperature of 130 K. The narrow peak shows the energy width of the incident He beam including all broadening by the instrument. The solid smooth curve is the theoretical fit with a surface temperature of 130 K and an effective end group mass of $M = 15$ amu.

implies that the results are well into the multiphonon regime with over 10 phonons transferred in a typical collision. (Note that the classical intensity of eq. (50) does not explicitly depend on the Debye–Waller factor, nevertheless $2W$ still exists and it can still be calculated.) This clearly explains the lack of quantum mechanical features in the data. At fixed incident energy and angle, the theoretical fit depends only on T and M; it does not depend on the Debye temperature. The position of the maximum in the inelastic intensity depends on $1/M$ through the energy shift ω_0, and the width of the inelastic intensity distribution varies as the ratio T/M. Thus the fit to the experimental data at known surface temperature gives a value of the effective mass of the end group of molecules from which the He projectiles scatter.

The ability to achieve a fit to the data with so few physical parameters implies, however, that very little can be learned about the fundamental dynamics of the surface vibrations from experiments carried out under these conditions. Instead, in order to learn the details of the surface dynamics, experiments must be carried out in the quantum mechanical limit. Such experiments are readily achievable even with the low mass Langmuir–Blodgett films of the present experiment. If the energy is lowered by a factor of 2 to around 15 meV and if the temperature is lowered to 40 K or below, conditions which are currently possible, then the value of the Debye–Waller exponent will be of order 4 implying that both diffraction and single phonon features should be resolvable. Use of other types of Langmuir–Blodgett or self assembly films with higher mass end groups present many possibilities for systems with strong quantum mechanical features [81,82].

9. Conclusions

We have presented in this review a treatment of the inelastic scattering of neutral atomic particles from surfaces which is particularly adapted to the description of multiphonon exchanges during the collision. Starting from very general principles of many-body scattering theory, we develop a formal treatment of the scattering problem. However, in order to have a theory tractable enough for calculations, a number of approximations must be made. We apply the trajectory approximation in order to make the connection with earlier treatments of similar problems. We apply a further approximation, called the quick collision approximation, which is particularly useful for carrying out calculations. The

quick collision approximation is based on the assumption that the multiphonon part of the scattering intensity is dominated by long wavelength and small frequency phonons.

The theory is developed in basically three different limits, fully quantum mechanical, semiclassical, and classical in order to be able to span the range of currently available experimental conditions which range from the quantum regime to classical scattering. In the process we show that the criterion which signals the onset of classical-like scattering behavior can be simply expressed in terms of the exponential argument of the Debye–Waller factor, namely $2W > 6$. Since $2W$ is a measure of the number of quanta exchanged in the scattering event, this criterion can also be expressed by saying that the onset of classical-like behavior, consisting of only multiquantum scattering, will occur when the average number of phonons exchanged in the collision becomes appreciably larger than 6.

We present several different calculations and compare them to recent experimental results in order to test the theory, and in particular to test the quick collision approximation. All experiments considered involve He scattering, but for surface systems covering the range from the alkali halide insulators, to metals, and the very interesting case of He scattering from a flat surface of a Langmuir–Blodgett film. These examples include conditions which vary from quantum mechanical to nearly classical. The good agreement achieved between theory and experiment shows that the diffuse multiphonon intensity in atom–surface scattering can be described with straightforward and tractable calculations. Furthermore, the comparisons with experiment support the two biggest approximations made in the calculations, (i) the use of the quick collision approximation, and (ii) the assumption that the multiphonon intensity does not depend strongly on the details of the phonon spectral density. However, the strong differences noticed in the shape and behavior of the multiphonon intensity from quite different surface systems, for example alkali halides and metals, demonstrate that the multiphonon intensity can provide important physical information on the nature of the atom–surface interaction potential.

Acknowledgements

The author would like to thank the Alexander von Humboldt foundation for support, and the Institut für Grenzflächenforschung und Vakuumphysik of the Forschungscentrum Jülich for hospitality during the course of this work. This work was supported by the NSF under grant No. DMR 9114015.

References

[1] O. Stern, Naturwissenschaften 17 (1929) 391.
[2] I. Estermann and O. Stern, Z. Phys. 61 (1930) 95.
[3] I. Estermann, R. Frisch and O. Stern, Z. Phys. 73 (1931) 348.
[4] R. Frisch and O. Stern, Z. Phys. 84 (1933) 430.
[5] J.M. Jackson and N.F. Mott, Proc. Roy. Soc. (London) Ser. A 137 (1932) 703.
[6] J.E. Lennard-Jones and C. Strachan, Proc. Roy. Soc. (London) Ser. A 150 (1935) 442.
[7] C. Strachan, Proc. Roy. Soc. (London) Ser. A 140 (1935) 456.
[8] J.E. Lennard-Jones and A.F. Devonshire, Nature 137 (1936) 1069.
[9] J.E. Lennard-Jones and A.F. Devonshire, Proc. Roy. Soc. (London) Ser. A 156 (1936) 6.
[10] J.E. Lennard-Jones and A.F. Devonshire, Proc. Roy. Soc. (London) Ser. A 156 (1936) 29.
[11] J.E. Lennard-Jones and A.F. Devonshire, Proc. Roy. Soc. (London) Ser. A 158 (1936) 242.
[12] J.E. Lennard-Jones and A.F. Devonshire, Proc. Roy. Soc. (London) Ser. A 158 (1936) 253.
[13] A.F. Devonshire, Proc. Roy. Soc. (London) Ser. A 156 (1936) 37.
[14] A.F. Devonshire, Proc. Roy. Soc. (London) Ser. A 158 (1937) 269.
[15] J.N. Smith, Jr., D.R. O'Keefe, H. Saltzburg, R.L. Palmer, J. Chem. Phys. 50 (1969) 4667.
[16] S.S. Fisher, M.N. Bishara, A.R. Kulthau and J.E. Scott Jr., Proc. 5th. Symp. Rarefied Gas Dynamics (1969), p. 1227.

[17] R.B. Subbarao and D.R. Miller, J. Chem. Phys. 51 (1969) 4679.
[18] B.R. Williams, J. Chem. Phys. 55 (1971) 1315.
[19] B.R. Williams, J. Chem. Phys. 55 (1971) 3220.
[20] N. Cabrera, V. Celli and R. Manson, Phys. Rev. Lett. 22 (1969) 396.
[21] A. Tsuchida, Surf. Sci. 14 (1969) 375.
[22] N. Cabrera, V. Celli, F.O. Goodman and R. Manson, Surf. Sci. 19 (1970) 67.
[23] H. Hoinkes, Rev. Mod. Phys. 52 (1980) 933.
[24] G. Boato and P. Cantini, Adv. Electron. Electron Phys. 60 (1983) 95.
[25] V. Bortolani and A.C. Levi, Rivista Nuovo Cimento 9 (1986) 1.
[26] J.A. Barker and D.J. Auerbach, Surf. Sci. Rep. 4 (1984) 1.
[27] T. Engle and K.H. Rieder, Springer Tracts Mod. Phys. 19 (1982) 1.
[28] R.B. Gerber, Chem. Rev. 87 (1987) 29.
[29] V. Celli, in Many Body Phenomena at Surfaces, eds. D. Langreth and H. Suhl (Academic, New York 1984) p. 315.
[30] J.P. Toennies, Physica Scripta T 19 (1987) 39.
[31] A. Lahee, J.R. Manson, J.P. Toennies and Ch. Wöll, Phys. Rev. Lett. 57 (1986) 471.
[32] C.W. Skorupka and J.R. Manson, Phys. Rev. B 41 (1990) 8156.
[33] B.J. Hinch and J.P. Toennies, Phys. Rev. B 42 (1990) 1209.
[34] A. Lahee, J.R. Manson, J.P. Toennies and Ch. Wöll, J. Chem. Phys. 86 (1987) 7194.
[35] V. Bortolani, V. Celli, A. Francini, J. Idiodi, G. Santoro, K. Kern, B. Poelsema and G. Comsa, Surf. Sci. 208 (1989) 1.
[36] J.R. Manson and V. Celli, Phys. Rev. B 39 (1989) 3605.
[37] V. Celli, D. Himes, P. Tran, J.P. Toennies, Ch. Wöll and G. Zhang, Phys. Rev. Lett. 66 (1991) 3160.
[38] J.L. Beeby, J. Phys. C 5 (1972) 3438.
[39] J.L. Beeby, J. Phys. C 5 (1972) 3457.
[40] A.C. Levi, Nuovo Cimento B 54 (1979) 357.
[41] A.C. Levi and H. Suhl, Surf. Sci. 88 (1979) 221.
[42] R. Brako and D.M. Newns, Phys. Rev. Lett. 48 (1982) 1859.
[43] R. Brako and D.M. Newns, Surf. Sci. 123 (1982) 439.
[44] M. Lagos, Surf. Sci. 65 (1977) 124.
[45] M. Lagos, Surf. Sci. 71 (1978) 414.
[46] B. Jackson, J. Chem. Phys. 88 (1988) 1383.
[47] B. Jackson, J. Chem. Phys. 92 (1990) 1458.
[48] H.D. Meyer and R.D. Levine, Chem. Phys. 85 (1984) 189.
[49] W. Brenig, Z. Phys. B 36 (1979) 81.
[50] J. Böheim and W. Brenig, Z. Phys. B 41 (1983) 243.
[51] David A. Micha, J. Chem. Phys. 74 (1981) 2054.
[52] D. Kumamoto and R. Silbey, J. Chem. Phys. 75 (1981) 5164.
[53] M. Jezercak, P.M. Agrawal, C. Smith and L.M. Raff, J. Chem. Phys. 88 (1988) 1264.
[54] R. Kosloff and C. Ceerjan, J. Chem. Phys. 90 (1989) 7556.
[55] B.H. Choi and R.T. Poe, J. Chem. Phys. 83 (1985) 1330.
[56] K. Burke, B. Gumhalter and D. Langreth, to be published.
[57] J.H. Jensen, L.D. Chang and W. Kohn, Phys. Rev. A 40 (1989) 1198.
[58] K. Burke and W. Kohn, Phys. Rev. B 43 (1991) 2477.
[59] J.G. Skofronick, G.G. Bishop, W.P. Brug, G. Chern, J. Duan, S.A. Safron and J.R. Manson, Superlattices and Microstructures 7 (1990) 239.
[60] Robert Weinstock, Phys. Rev. 65 (1944) 1.
[61] R. Glauber, Phys. Rev. 87 (1952) 189.
[62] R. Glauber, Phys. Rev. 98 (1955) 1962.
[63] L. Van Hove, Phys. Rev. 95 (1954) 249.
[64] Leonard S. Rodberg and R.M. Thaler, Quantum Theory of Scattering (Academic, New York, 1967).
[65] V. Celli, D. Himes and J.R. Manson, to be published.
[66] J.R. Manson, Phys. Rev. B 43 (1991) 6924.
[67] D. Himes and V. Celli, Surf. Sci. 272 (1992) 139.
[68] J.G. Skofronick, G.G. Bishop, W.P. Brug, G. Chern, J. Duan, S.A. Safron and J.R. Manson, Superlattices and Microstructures 7 (1990) 239.
[69] S.A. Safron, W.P. Brug, G. Chern, J. Duan, J.G. Skofronick and J.R. Manson, J. Vac. Soc. Tech. A 8 (1990) 2627.
[70] G.G. Bishop, W.P. Brug, G. Chern, J. Duan, S.A. Safron, J.G. Skofronick and J.R. Manson, Phys. Rev. B., in press.
[71] J.R. Manson and J.G. Skofronick, to be published.

[72] E. Hulpke, Surf. Sci. 52 (1975) 615.
[73] U. Gerlach-Meyer and E. Hulpke, Chem. Phys. 22 (1977) 325.
[74] J. Beeby, J. Phys. C 4 (1971) L359.
[75] R.I. Masel, Surf. Sci. 77 (1978) L179.
[76] J.R. Manson and G. Armand, Surf. Sci. 184 (1987) 511.
[77] V. Celli, G. Benedek, U. Harten, J.P. Toennies, R.B. Doak and V. Bortolani, Surf. Sci. 143 (1984) L376.
[78] F.O. Goodman and H.Y. Wachman, Dynamics of Gas–Surface Scattering (Academic, New York, 1976).
[79] V. Vogel and Ch. Wöll, J. Chem. Phys. 84 (1986) 5200.
[80] V. Vogel and Ch. Wöll, Thin Solid Films 159 (1988) 429.
[81] C.E.D. Chidsey, G.-Y. Liu, P. Roundtree and G. Scoles, J. Chem. Phys. 91 (1989) 4421.
[82] P. Fenter, P. Eisenberger, J. Li, N. Camillone, S. Bernasek, G. Scoles, T.A. Ramanarayanan and K.S. Liang, Langmuir 7 (1991) 2013.

84) p. 315.

. 208 (1989) 1.

; and Microstructures

; and Microstructures

1990) 2627.
B., in press.